Journal of Bio- and Tribo-Corrosion (2021) 7:68
https://doi.org/10.1007/s40735-021-00500-z

Electrochemical Noise and Polarization Analyses on Corrosion of Al-Brass Alloy During Erosion-Corrosion

M. Abedini[1,2] · H. M. Ghasemi[1]

Received: 17 November 2020 / Revised: 1 March 2021 / Accepted: 2 March 2021 / Published online: 27 March 2021

Abstract
It is known that impingement of solid particles on the surface of alloys could cause an increase in corrosion rate during erosion-corrosion. The increase in corrosion rate by erosion could be studied using the common electrochemical technique of polarization. Electrochemical noise method, on the other hand, has been widely used to study the localized corrosion. This technique could provide useful data on the effect of single particle impact on the corrosion rate of materials. In the present paper, both techniques of polarization and electrochemical noise were used to study the corrosion behavior of Al-brass alloy during erosion-corrosion. The erosion-enhanced corrosion rate was calculated and the results obtained from these two techniques were compared. The erosion-corrosion tests were performed at various sand concentrations of 0–30 g/l and different particle sizes. Under sand concentrations lower than 10 g/l, the electrochemical noise technique as a proper method for analysis of localized corrosion showed higher accuracy in measuring the erosion-enhanced corrosion as compared with the polarization method. However, at the concentrated slurries, higher possibility of simultaneous impacts and, therefore, overlapping of the current peaks imposed some limitation for the electrochemical noise method. The polarization and noise analyses revealed that an increase in the particle size resulted in an increase up to 2.8 times in the erosion-enhanced corrosion rate of the alloy.

Keywords Erosion-corrosion · Al-brass · Electrochemical noise · Polarization

1 Introduction

Erosion-corrosion refers to surface damage encountered by components exposed to a corrosive fluid stream containing solid particles. Particle impacts on the surface of materials result in material removal through erosive wear, i.e., mechanical damage. The impingement of particles on the surface could also increase the corrosion rate during slurry erosion. The combined actions of electrochemical corrosion and mechanical erosion could accelerate the materials degradation [1, 2]. Therefore, it is necessary to investigate the effect of erosion on corrosion behavior of alloys to understand the exact damage mechanism and to investigate the possibility of life enhancement of components.

✉ H. M. Ghasemi
hghasemi@ut.ac.ir

[1] School of Metallurgy and Materials Engineering, College of Engineering, University of Tehran, Tehran, Iran

[2] Department of Metallurgy and Materials Engineering, Faculty of Engineering, University of Kashan, Kashan, Iran

Electrochemical impedance spectroscopy and polarization techniques are two most common methods for obtaining the erosion-enhanced corrosion rates of various metals and alloys [3–9]. However, these two methods could not detect the localized effect of particle impacts on the corrosion behavior during the erosion-corrosion [10]. On the other hand, electrochemical noise analysis as a non-destructive technique has been successfully used for detection and analysis of localized corrosion processes in the recent years [11, 12]. During a corrosion process, the cathodic and the anodic reactions can cause minute transients in the electrical charges that manifest in the form of current and potential noise. In the electrochemical noise method, the fluctuations of current and potential are recorded and the results can be used to detect the corrosion type [13–16] and obtain the corrosion rate [14, 17]. The electrochemical noise analysis consists of the current noise between two nominally identical working electrodes and the potential noise between these electrodes and a reference electrode [13, 18–22]. However, in the previous studies on the corrosion behavior of materials during erosion-corrosion by the electrochemical noise

method [23–26], the current variations were measured between a working electrode (which was under erosion) and a counter electrode (graphite and platinum). In this mode of analysis, the galvanic corrosion between the working and counter electrodes may accelerate the erosion-enhanced corrosion rate of the samples [27].

The effect of particle diameter and jet velocity on the current transient of 304L stainless steel during erosion-corrosion was investigated by Burstein and Sasaki [23]. They found a linear increase in the current peak with the impact energy which was determined by particle velocity and particle mass. Rajahram et al. [24] have investigated electrochemical noise of stainless steel UNS S31603 under the erosion-corrosion using a slurry pot. They reported that increasing the impact velocity and sand concentration would increase the average current noise level. Generated noise by a single particle impact was also investigated by Rajahram et al. [24]. The current transient occurred over a very short period of time between 18 and 39 ms with a higher magnitude at the higher impact velocities.

Wood et al. [28] have observed a higher amplitude oscillations in the erosion-corrosion tests of AISI 304L stainless steel as compared with the flow condition, i.e., no sand concentration using noise measurements. This was attributed to the active surfaces generated due to the particle impacts, which resulted in erosion-enhanced corrosion. Mohammadi et al. [26] studied the current transient induced by single particle impingement on the surface of a passivated 304 stainless steel using noise measurements. The current due to the particle impingement at various sand concentrations was calculated by the sum of electric charge created by individual impacts. At low sand concentrations up to 1 wt% (i.e., 10 g/l) the calculated data were very close to the experimental values. However, at the higher sand concentrations the calculated current prediction showed a higher value than the experimental current which was attributed to the particle interactions at the higher sand concentrations.

Aluminum–brass (Al–brass) alloy as an erosion-corrosion resistant material has been extensively used in condensers and heat exchangers. In these applications, the alloy is exposed to both mechanical erosive wear and electrochemical corrosion. Therefore, study of the erosion and corrosion of the alloy could help better understanding of mechanisms of material removal during erosion-corrosion. The pure erosion, pure corrosion, erosion-corrosion and synergism between erosion and corrosion of the alloy have been studied recently [5, 10]. The highest erosion-corrosion and pure erosion rates were obtained at an impingement angle of 40°. Effect of jet velocity and sand concentration on the corrosion behavior of the alloy under slurry erosion was studied using the polarization and electrochemical impedance spectroscopy (EIS) techniques and an equation was obtained to predict the erosion-enhanced corrosion rate of the alloy [10]. It was concluded that the polarization method may not be a proper method to measure the corrosion rate of the alloy under slurry erosion at low sand concentrations. Another study showed that the formation of ripples on the surface of pure erosion samples under oblique angles could lead to a large increase in the average surface roughness of the Al-brass samples [29].

Though, both polarization and electrochemical noise techniques have been wildly used to study the corrosion behavior of various alloys under erosion-corrosion, however, it is not clear whether the obtained results from these two methods could verify each other. Moreover, the possible limitations of these two methods for measuring the erosion-enhanced corrosion in various sand concentrations are not well addressed in the literature. Therefore, a comparison of polarization and electrochemical noise results could provide useful data to discuss the advantages and disadvantages of the methods for measuring the corrosion rate of alloys in erosion-corrosion process.

In the present paper, the effect of sand concentration and particle size on the erosion-enhanced corrosion behavior of Al-brass alloy was investigated. The use of electrochemical noise and polarization methods were compared to discuss the effect of particle impacts on the corrosion behavior of the alloy. To remove or decrease the galvanic effects, the electrochemical noise tests were performed on two identical working electrode mode, i.e., two identical samples under impingement during erosion-corrosion.

2 Experimental Procedure

Al-brass alloy with a composition of Cu-19.2%Zn-2.3%Al-0.1%As was used as the target material. The cast ingots were solution annealed at 750 °C for 4 h, cold rolled into a thickness of 8 mm (an about 42% reduction) and finally, annealed at 550 °C for 2 h. The hardness of the alloy was about 75 Hv. Cylindrical samples were wire-cut and the erosion surface was ground to an average surface roughness (R_a) of about 0.1 µm measured by a stylus surface profilometer (Model T8000, Hommelwerke, Germany). The erosion-corrosion tests were performed in a slurry impingement rig designed and built by the authors. The details of the rig have been described elsewhere [3]. The container, nozzle, tubes, connections, and the pumping impellers were all made of non-conductive materials to avoid any interference with the electrochemical measurements. The normal distance between the nozzle tip and the surface of the samples was fixed to 5 mm in all experiments. A shielded cable was soldered to the back side of each sample, and the joint region was covered with a non-conductive polymer. The surfaces except the erosion side were then coated with lacquer and placed in the sample holder. Polymeric holders were used to fix the samples under

the nozzle. The erosion-corrosion tests were performed in 3.5 wt% NaCl solution containing SiO_2 particles with a size of 318 ± 20 µm at various sand concentrations of 0–30 g/l. The tests were carried out at a jet velocity of 6 m/s under normal impingement angle. To study the effect of particle size on the erosion-enhanced corrosion behavior of the alloy, the erosion-corrosion tests were also performed in the presence of SiO_2 particles with average sizes of 260 ± 12 and 528 ± 30 µm. The morphology of the SiO_2 particles with the sizes of 260 ± 12 and 528 ± 30 µm is shown in Fig. 1. It should be mentioned that SiO_2 particles with various sizes were obtained by sieving silica casting sand.

The corrosion rate of the alloy during erosion-corrosion tests was measured using two electrochemical techniques of polarization and noise. A same slurry impingement rig was used for both polarization and noise measurements. The electrochemical measurements were performed using a 302 N Autolab potentiostat/galvanostat (Metrohm, Netherlands) with NOVA 1.9 associated software. In the polarization tests, a sample with a diameter of 5 mm was mounted on the sample holder and placed under the nozzle as schematically shown in Fig. 2a. The counter and reference electrodes were graphite and saturated Ag/AgCl in a capillary, respectively. The capillary was used to place the reference electrode as close as possible to the working electrode providing more accuracy in the electrochemical measurements, i.e., to minimize the error due to IR drops [30]. The polarization curves were obtained by scanning the applied potential

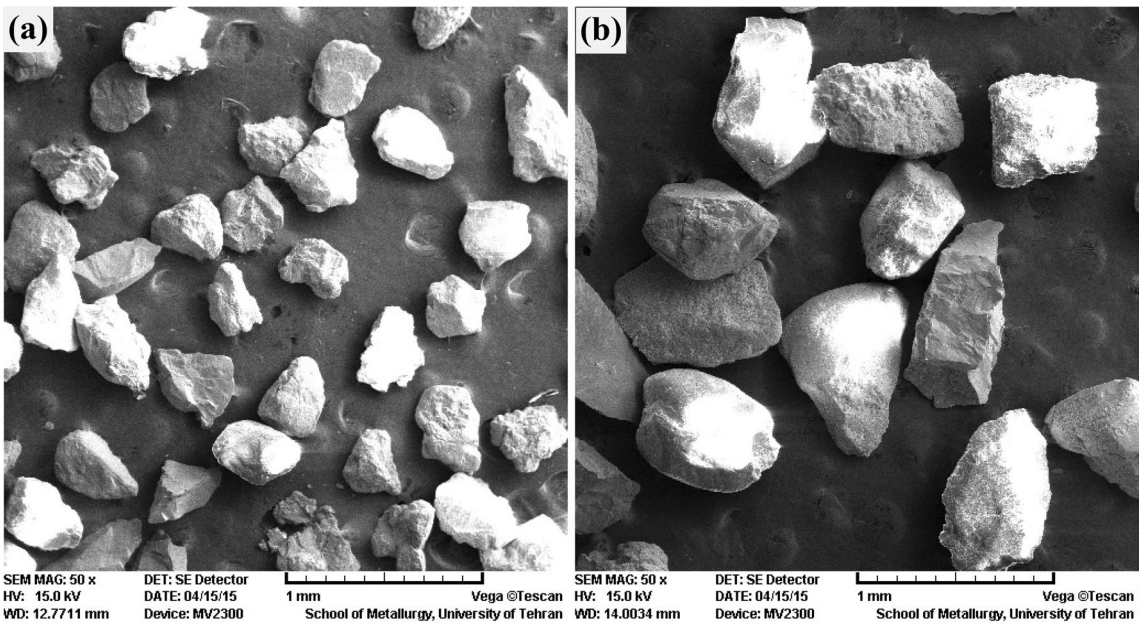

Fig. 1 The morphology of the eroding particles with two sizes of: **a** 260 ± 12 µm and **b** 528 ± 30 µm

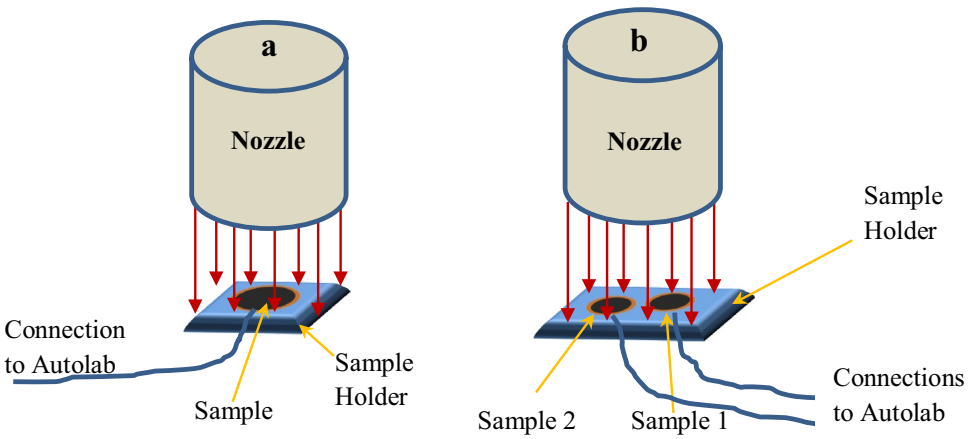

Fig. 2 Schematics showing the positioning of the samples under the nozzle in: **a** polarization and **b** noise measurements

from − 200 to + 700 mV versus open circuit potential (OCP) at a scan rate of 2 mV/s during the erosion-corrosion. The corrosion current densities were then obtained by Tafel extrapolation method.

In the electrochemical noise measurements, two identical samples, 2.6 mm in diameter, were exposed to the slurry impingement and connected to the noise modulus of the potentiostat as shown in Fig. 2b. The position of two samples was symmetrical to the centerline of the nozzle to provide a uniform flow across the samples. The current noise between two samples was recorded during the erosion-corrosion tests for 64 s at an acquisition rate of 400 Hz at the open circuit potential. The current was monitored using ECN (i.e., electrochemical noise) module of the potentiostat to gain the highest resolution in measurements. To minimize the extraneous noise from the surrounding environment in the system, the erosion-corrosion container was enclosed in an aluminum earth-grounded Faraday cage. Shielded wires were used for the connections between the samples and the potentiostat. Finally, the eroded surfaces were examined using a scanning electron microscope (SEM, Tescan, Czech Republic).

3 Results and Discussion

3.1 Noise Analysis of Single Particle Impact

Figure 3 shows a typical current–time curve of Al-brass alloy obtained by the electrochemical noise method during the erosion-corrosion at a sand concentration of 0.1 g/l, particle size of 528 µm, jet velocity of 6 m/s and impingement angle of 90°. To show the transient current peaks in more details, the curve was depicted for only 3 and 0.1 s in Fig. 3a and b, respectively. A periodic background signal with a period of 20 ms and a peak-to-peak amplitude of the order of 0.2 µA could be observed in the figure. The frequency of background signals was 50 Hz, which was attributed to the external electrical fields generated by the electrical power line. Some well-defined transient current peaks were also observed at both positive and negative directions in the current–time curve in Fig. 3a. The opposite transient peaks were attributed to the impingement of the particles on samples 1 and 2 (Fig. 2b) during the erosion-corrosion.

Figure 4 shows SEM micrographs of the eroded surface after 64 s of erosion-corrosion at a jet velocity of 6 m/s in the presence of 0.1 g/l SiO_2 particles with a size of 528 µm. A low concentration impact at a short time could simulate the impact of a single particle. The impact of particles under an impingement angle of 90° could induce indentation as shown in Fig. 4b. These impacts resulted in removal of material from the surface in the form of erosive wear and generation of a bare metal surface that would be further exposed to

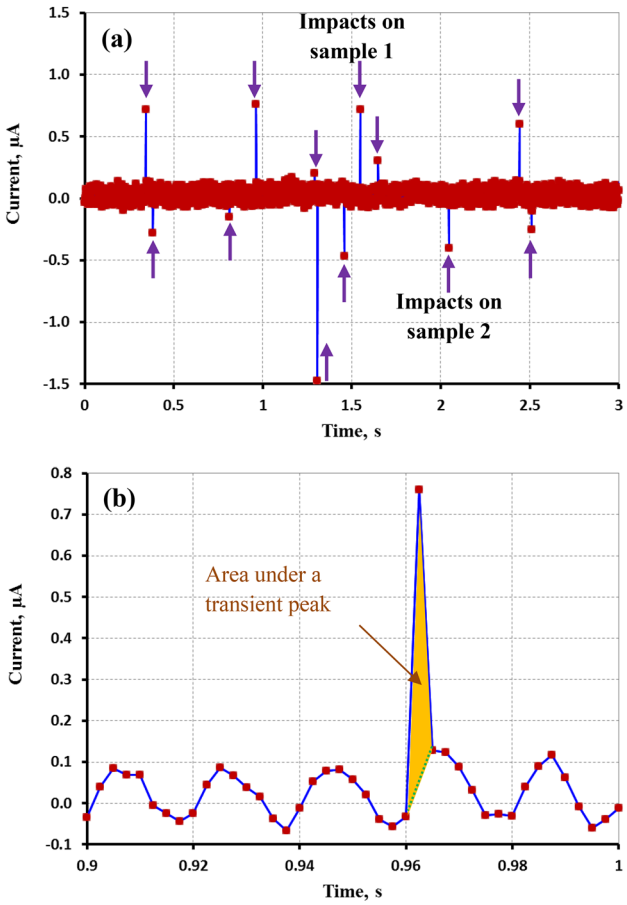

Fig. 3 A typical current–time curve of Al-brass alloy obtained by the electrochemical noise method indicating the well-defined transient peaks due to the particle impacts during erosion-corrosion at sand concentration of 0.1 g/l, particle size of 528 µm, jet velocity of 6 m/s, and impingement angle of 90° for: **a** 3 s and **b** 0.1 s

the corrosive medium. The electrochemical reactions occurring on these sites could generate some electrical charges on the surface of the sample, which appeared as the transient current peaks in the current–time curve in Fig. 3. Moreover, the impingement of a single particle may induce some plastic deformation in the impacted region as shown in Fig. 4c. This was also resulted in the formation of fine deformed lips on the eroded surfaces. The subsequent impacts of the particles could cause more plastic deformation on the surface, and finally detach the deformed lips resulting in mechanical erosive wear. The plastic deformation of the surface could also momentarily increase the activity of the material and, therefore, cause a sharp increase in the corrosion current of one sample respect to the other, inducing the transient peaks in the current–time curve in Fig. 3.

Figure 4a shows that the maximum number of impacts with a detectable deformation on a surface area of 81,225 μm^2 (i.e., the apparent area of the image in Fig. 4a) was 14 after 64 s of impingement during the electrochemical noise

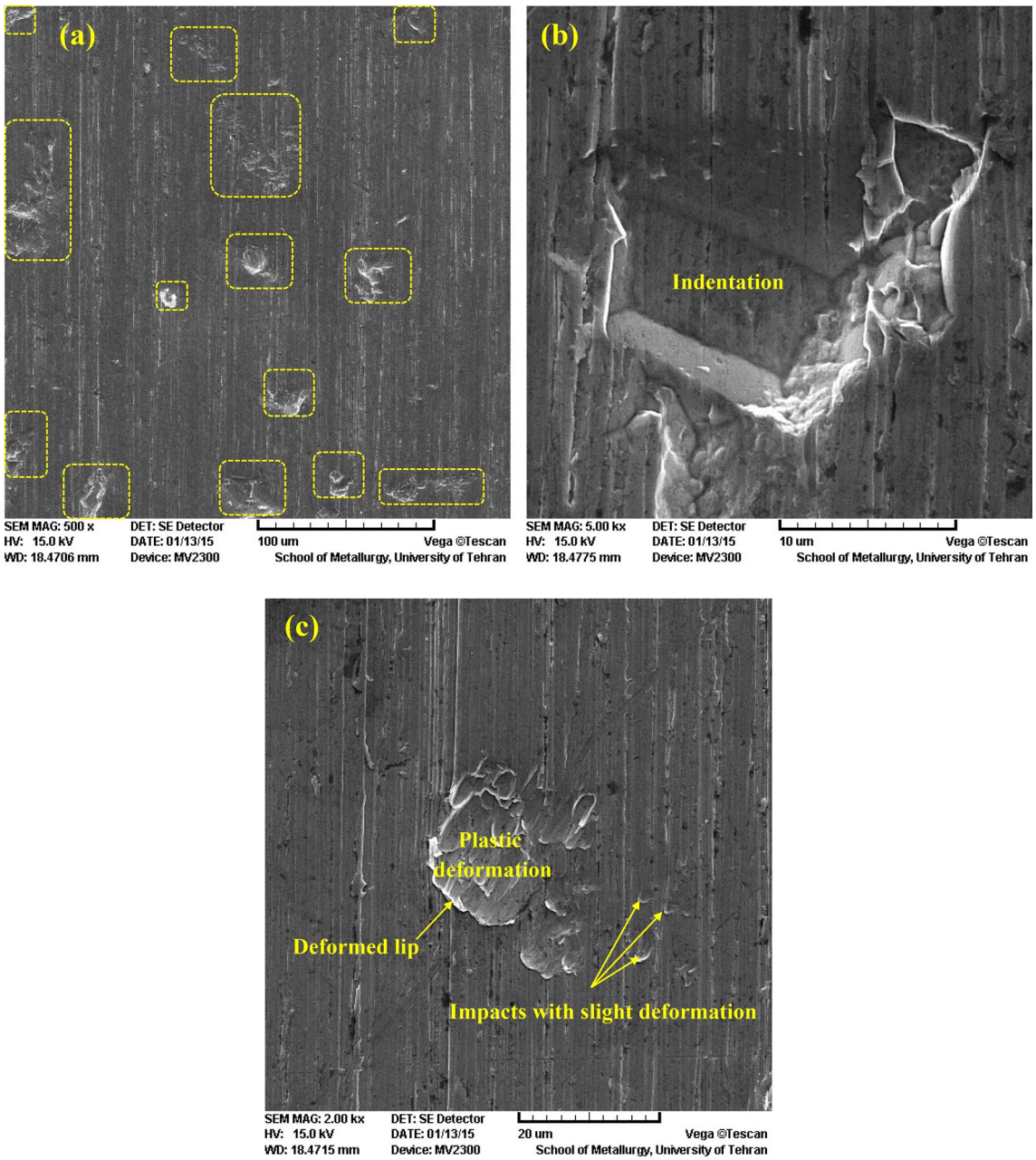

Fig. 4 SEM micrographs of surface of Al-brass alloy after 64 s erosion-corrosion at a jet velocity of 6 m/s under normal impingement at the presence of 0.1 g/l SiO_2 particles with size of 528 µm: **a** at a low magnification, in which the rectangles indicate the regions of the impacts, and **b**, **c** at higher magnifications showing the indentation and plastic deformation of the surface

measurement. Assuming a uniform particle impingement on the entire eroded surface could suggest about 1000 impacts on the surface of each sample with a surface area of 5.3 mm^2 (i.e., a sample diameter of 2.6 mm) after 64 s. The number of impacts could also be calculated by theoretical calculation that was described in Reference [10]. The theoretical number of impacts on the surface of each sample after 64 s was calculated to be about 1050 which was close to the number of impacts obtained by the analysis of the eroded surface. However, Fig. 3a shows that the total number of detectable transient current peaks in a period of 3 s of the noise curve was 12 indicating an average of 6 impacts on the surface of each sample. Therefore, the total number of impacts on the surface of each sample after 64 s would be about 128 that was about one eighth of the number of impacts obtained by the theoretical calculations [5] and examination of the eroded surface in Fig. 4a. It seems that the removal of the corrosion products, i.e., mainly copper oxides [31], and the

amount of plastic deformation induced by the majority of particle impacts were not large enough to obtain a remarkable rise in the corrosion current. Some typical plastic deformation sites induced by the impingement of particles are shown in Fig. 4c. Some impact sites were slightly deformed, which did not result in transient current peaks larger than 0.1 µA, i.e., the periodic background signals [25, 28] in Fig. 3b. Therefore, the number of counted transient current peaks in the current–time curves was inevitably lower than the actual number of particle impacts.

3.2 Effect of Sand Concentration

Figure 5 shows the current–time curves of Al-brass alloy obtained by the electrochemical noise measurements in the stagnant and erosion-corrosion tests at a jet velocity of 6 m/s and various sand concentrations (particle size of 318 µm) under an impingement angle of 90°. The details of the instantaneous changes in the currents during stagnant (Fig. 5a), the flow, i.e., 0.0 g/l, and a low sand concentration of 0.1 g/l (Fig. 5b, and c) are also presented at the top right corner of the figures. Under the stagnant and flow conditions, a periodic signal pattern that consisted of repetitive current–time trace with no impact features could be observed in Fig. 5a and b. This revealed that the specimens were undergoing uniform corrosion [32], i.e., no localized corrosion occurred on the surface of Al-brass alloy at the stagnant and flow conditions. At a sand concentration of 0.1 g/l, well-defined transient current peaks with a maximum amplitude of about 0.5 µA was observed at both positive and negative directions in the current–time curve in Fig. 5c. These peaks could be as a result of localized corrosion that occurred at the impact regions on both samples. Figure 5 shows that the frequency and amplitude of the current transient peaks were increased as the sand concentration increased. The probability of simultaneous impacts on

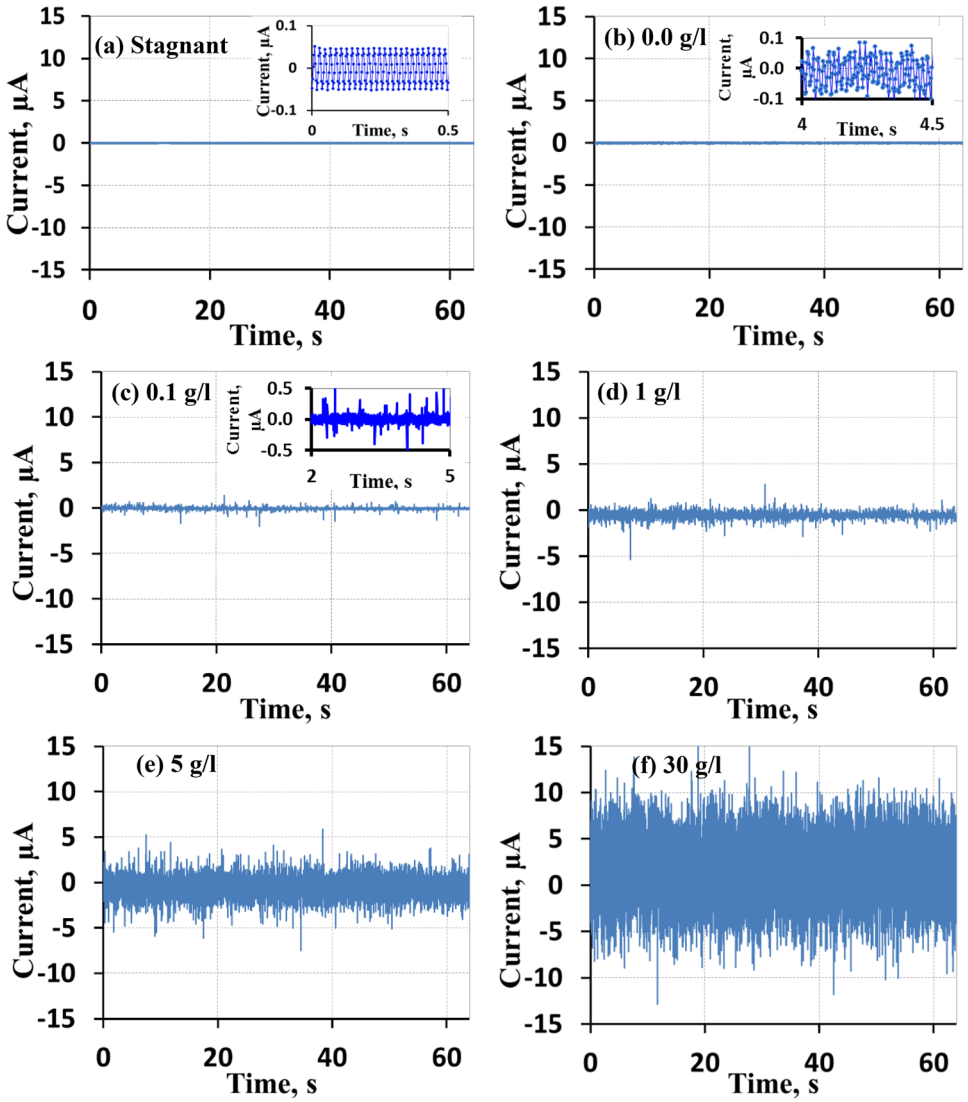

Fig. 5 The current–time curves of Al-brass alloy obtained by the electrochemical noise method in stagnant (**a**) and erosion-corrosion tests at a jet velocity of 6 m/s, impingement angle of 90°, particle size of 318 µm and various sand concentrations of: **b** 0.0 g/l, **c** 0.1 g/l, **d** 1 g/l, **e** 5 g/l, and **f** 30 g/l

the surface of a sample could be increased as the sand concentration increased. This could induce a larger plastically deformed area and, therefore, a larger bare area exposed to corrosive medium. This resulted in a significant increase in the amplitude of the current transients, which reached to a maximum of about 10 µA at a high sand concentration of 30 g/l compared to 0.5 µA for a sand concentration of 0.1 g/l.

Since multiplying the current by time gives the related charge ($Q = it$), the area under each current peak in the current–time curves typically shown in Fig. 3b could represent the charge generated by a single particle impact and/or simultaneous impacts. The average electrical charge, i.e., the average area under the detectable peaks, for various sand concentrations in Fig. 5 is shown in Fig. 6. Since the energy of particles would not change with sand concentration, a similar mean electrical charge was expected at all sand concentrations. However, Fig. 6 reveals that increasing the sand concentration from 0.1 to 30 g/l increased the average electrical charge of the current peaks from 1 to 37 nC. This was attributed to the higher probability of higher amplitude peak generation due to the simultaneous impacts and, therefore, a larger area under the peaks at the higher sand concentrations.

Peak search was also performed on the data of Fig. 5 using the NOVA 1.9 software and the numbers of detectable peaks in the current–time curves were obtained at both positive and negative directions. The sums of the number of peaks at both directions (i.e., on both samples) for various sand concentrations are shown in Fig. 6. It should be mentioned that the number of counted transient current peaks in Fig. 6 were inevitably lower than the theoretical number of impacts [10] as discussed in the previous section. Figure 6 shows that increasing the sand concentration up to 3 g/l led to an increase in the number of counted peaks, a trend that was expected due to the higher frequency of impacts at the higher sand concentrations. Further increase in the sand concentration from 3 to 30 g/l caused no remarkable change in the number of counted peaks. The current peaks generated by simultaneous impacts on the surface of a sample would overlap and they were detected as a single peak in the current–time curves. Since the increase in the sand concentration would raise the probability of the simultaneous impacts, larger peaks instead of higher number of peaks could be observed at the concentrated slurries in Fig. 6. It is also possible that the simultaneous impacts on both samples could result in the damping or annihilation of the current peaks at opposite directions leading to a peak with a low or zero magnitude in Fig. 5. This could be another reason for the constant current peaks counted at the sand concentrations higher than 3 g/l in Fig. 6.

The polarization curves of Al-brass alloy during the erosion-corrosion tests at a jet velocity of 6 m/s, impingement angle of 90°, particle size of 318 µm and various sand concentrations are shown in Fig. 7. The figure shows that the corrosion potential decreased (i.e., higher corrosion tendency) as the sand concentration increased especially for the sand concentrations of 10 g/l and higher. The polarization curves were also shifted to higher current densities as the sand concentration increased indicating a higher corrosion rate at the higher sand concentrations. These could be related to the higher removal rate of any corrosion products formed [22] and higher plastic deformation and work-hardening of the eroded surface at the concentrated slurries that provide higher corrosion tendency and rate.

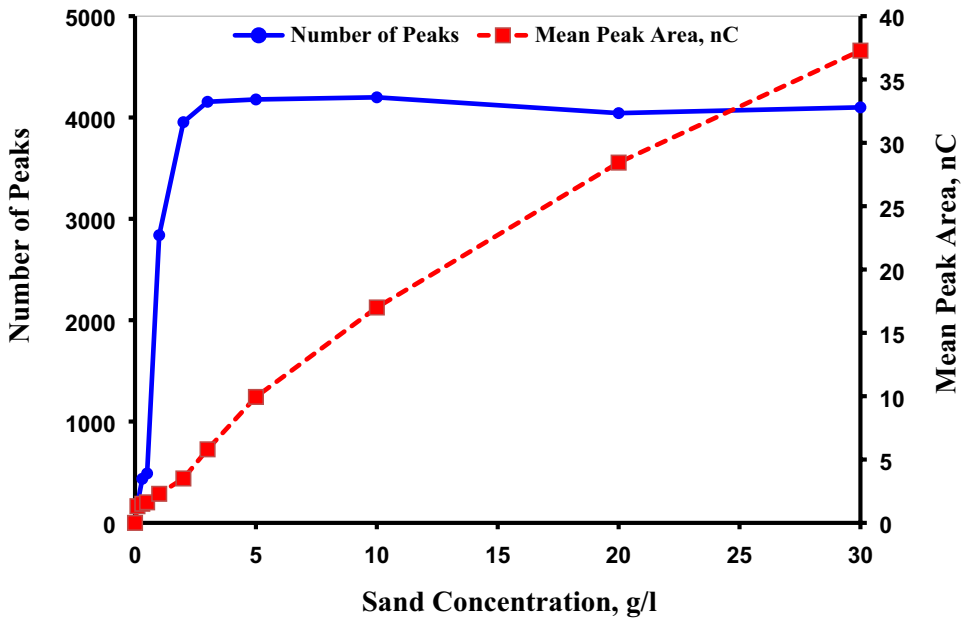

Fig. 6 The number of current peaks and the average charge of each peak obtained from the current–time curves of Al-brass alloy in Fig. 5 using the electrochemical noise measurements during erosion-corrosion for 64 s at a jet velocity of 6 m/s, impingement angle of 90°, and particle size of 318 µm as a function of sand concentration

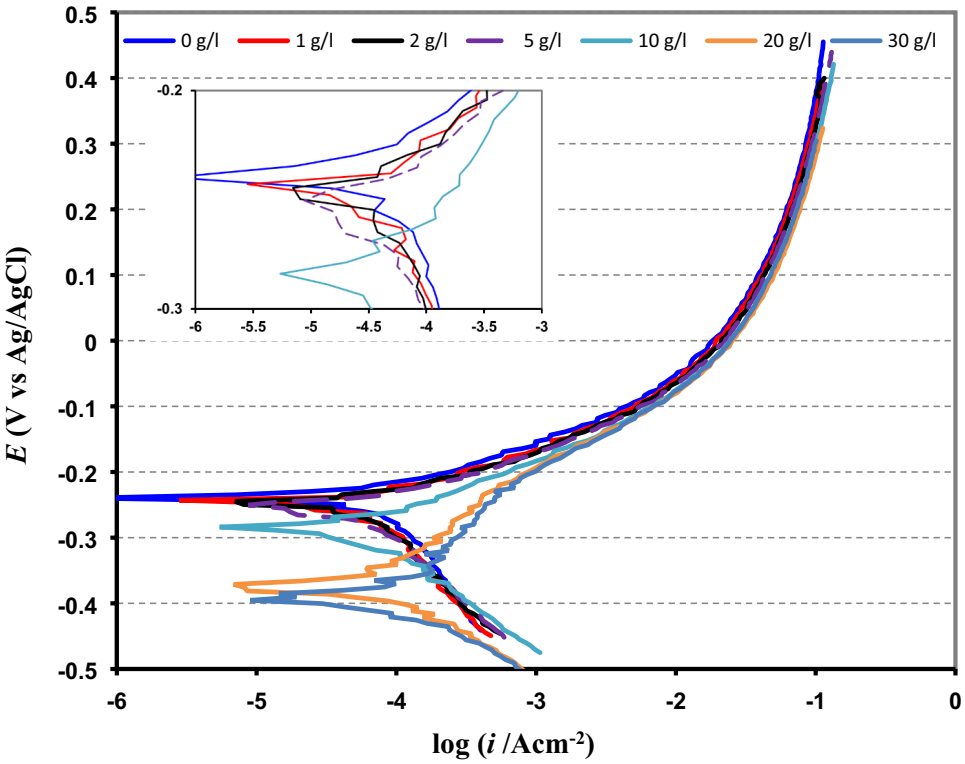

Fig. 7 Polarization curves of Al-brass alloy during the erosion–corrosion process at an impingement angle of 90°, jet velocity of 6 m/s and various sand concentrations with a particle size 318 µm. A closer observation of the curves at sand concentrations of 0–10 g/l is also presented in the figure as the inset

The corrosion current density at various sand concentrations was measured by Tafel extrapolation method. The increase in the current density (ΔC_w) due to the particle impacts was calculated by subtracting the corrosion current density at a sand concentration of 0.0 g/l or the flow test, i.e., 54 µA/cm^2, from the current densities under the loaded slurries. The values of erosion-enhanced current densities (ΔC_w), i.e., the change in corrosion due to erosion are presented in Fig. 8. On the other hand, the total current induced by the particle impacts in noise data of Fig. 5 could be also considered as the erosion-enhanced corrosion (i.e., ΔC_w). Indeed, the summing of the area under all detectable current peaks in Fig. 5 gives the overall charges generated by the impacts during the testing time. The total current induced

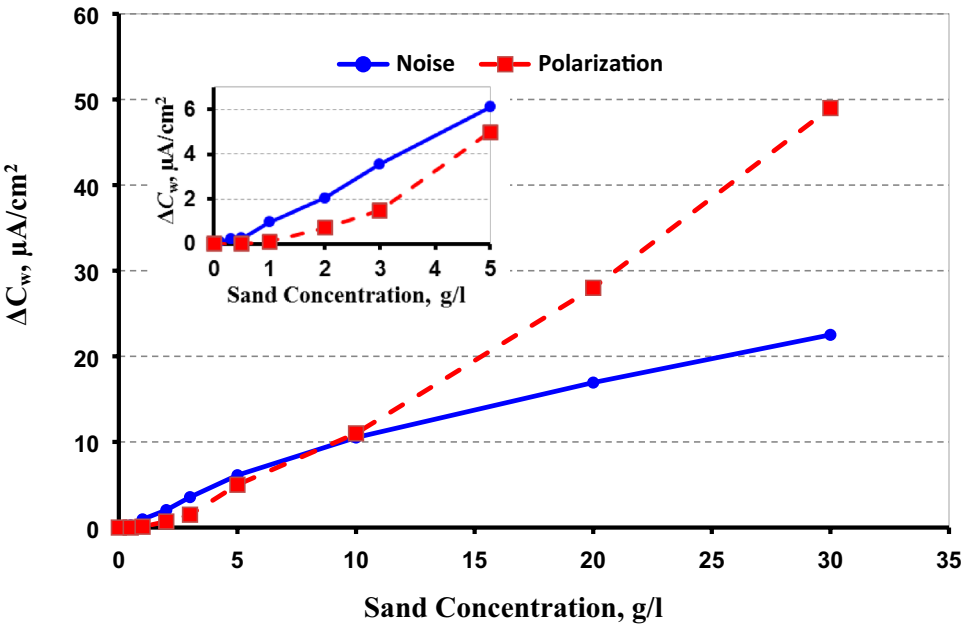

Fig. 8 Erosion-enhanced corrosion current density (ΔC_w) of Al-brass alloy obtained from electrochemical noise and polarizations methods during erosion-corrosion at a jet velocity of 6 m/s, impingement angle of 90° as a function of sand concentration with a particle size 318 µm. A closer observation of the curves at low sand concentrations is also presented in the figure as the inset

by the impacts on the eroded surface (ΔC_w) were obtained by dividing the overall charge by the testing time, i.e., 64 s, and the results are included in Fig. 8. Figure 8 indicates that the current densities obtained by both polarization and noise methods were increased as the sand concentration increased. This was expected due to the higher number of impacts on the surface at the higher sand concentrations [10]. In general, the increase in corrosion rate due to the impingement of particles (i.e., ΔC_w) could be attributed to four main mechanisms [5]: (I) removal of surface oxide layers and corrosion products that exposed the bare metal to the corrosive solution, (II) increasing the mass transport of oxygen that affects the concentration polarization, (III) rising the crystallographic defect density of surface layers due to the plastic deformation, and (IV) increasing the effective surface area due to the plastic deformation and formation of indentations and raised lips on the surface (Fig. 4). As the sand concentration increased, the frequency of particles impacts on the surface increased and, therefore, a higher corrosion rate was obtained through the abovementioned mechanisms.

Under the sand concentrations higher than 10 g/l, Fig. 8 shows that the current densities obtained from the noise measurements were lower than those obtained by Tafel method. This could be related to increasing the possibility of simultaneous impacts on the surfaces of samples 1 and 2 during the noise measurement at higher sand concentrations as discussed earlier. Since the currents obtained from these impacts were generated at the same time at opposite directions, they were not detected by the potentiostat. This resulted in an erosion-enhanced corrosion lower than expected under the sand concentrations higher than 10 g/l obtained by the electrochemical noise technique. It could be suggested that the electrochemical noise method is not an accurate technique for measuring the corrosion rate of alloys during the erosion-corrosion process at the concentrated slurries. This was also reported by Mohammadi et al. [26]. They used electrochemical noise technique to measure the charge induced by a single particle and estimated the corrosion current during erosion by multiplying the obtained charge by the number of impacts. At very low sand concentrations up to 10 g/l, the experimental values obtained from electrochemical noise measurements was very close to the calculated data. However, at higher sand concentrations, the experimental values were lower than the predicted values that was attributed to the interaction of particle impacts at the concentrated slurries.

A remarkable point in Fig. 8 is that at the sand concentrations lower than 10 g/l, the erosion-enhanced corrosion current densities obtained by the noise analysis were higher than the currents obtained by Tafel method. Figure 7 shows that there was no remarkable change between the polarization curves at the sand concentrations between 0 and 5 g/l. Due to the low frequency of impacts at the low sand concentrations, and therefore, lower removal rate of corrosion products and lower work hardening of the surface, the impingement of particles did not have a remarkable effect on the total corrosion behavior of the alloy [10]. As the sand concentration decreased, the frequency of impacts decreased linearly, so the decrease in the corrosion rate was expected to follow a linear trend. Figure 8 shows that this may be true for the sand concentrations higher than 10 g/l. At sand concentrations lower than 5 g/l, however, a nonlinear trend in ΔC_w was observed specially for the data obtained by the polarization method. In comparison with the electrochemical noise method as a suitable technique for detecting the localized corrosion [20] as for each impact, the polarization technique could only detect the total corrosion rate of the surface. The polarization method was not able to detect the effect of particle impacts on the corrosion behavior of the alloy at low sand concentrations. Therefore, at the sand concentration up to 5 g/l, the corrosion current densities obtained by the polarization method were lower than the values obtained by the noise analysis as shown in Fig. 8. The low accuracy of polarization technique for measuring the erosion-enhanced corrosion in dilute slurries were discussed in more details in another published paper [10].

The electrochemical noise technique, which showed some limitations in measuring the erosion-enhanced corrosion in the concentrated slurries, could be a proper method for measuring the corrosion rate during the erosion-corrosion at low sand concentrations. There might also be some non-detectable peaks in the current–time curves in Fig. 5 due to simultaneous impacts, which could result in higher values of the erosion-enhanced corrosion under low sand concentrations from the noise measurements in Fig. 8. However, despite this probable error in the noise results, the corrosion rates obtained from the noise analysis was higher than the polarization method at the low sand concentrations. This suggested the noise technique as a more precise method for measuring the corrosion rate during erosion-corrosion at the low sand concentrations.

3.3 Effect of Particle Size

To study the effect of particle size on the corrosion rate of the alloy during erosion-corrosion, the current–time curves during erosion-corrosion at a jet velocity of 6 m/s under impingement of SiO_2 sands with two particle sizes of 260 µm and 528 µm were obtained using electrochemical noise technique. The current–time curves at a sand concentration of 0.1 g/l for 60 s are typically shown in Fig. 9. The number of the peaks obtained from the noise data and the theory [10] and the calculated average area under each peak are also included in the figure. Increasing the particle size increased the peak amplitude and lowered the number of well-defined transient peaks from 320 for particle size of

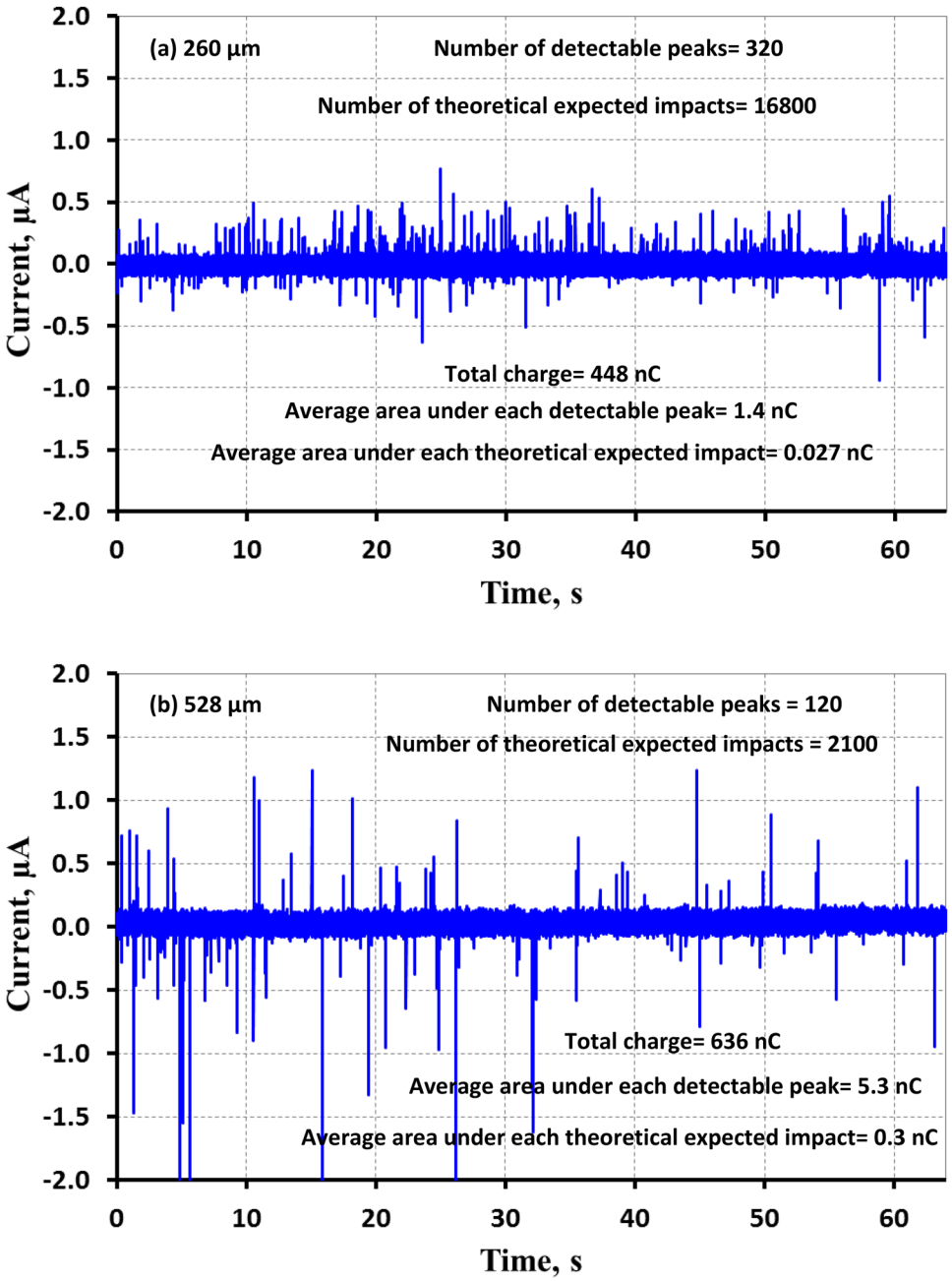

Fig. 9 Current–time curves of Al-brass alloy obtained by electrochemical noise method during the erosion-corrosion at a jet velocity of 6 m/s, impingement angle of 90°, sand concentration of 0.1 g/l and particle sizes of: **a** 260 µm and **b** 528 µm

260 µm to 120 for particle size of 528 µm in Fig. 9. With increasing the diameter of the particles by about two times, the volume of each particle would increase by almost eight times and, therefore, at a constant sand concentration, the number of particles would be lowered by one eighth. This resulted in an eightfold increase in the theoretical number of impacts from 2100 to 16,800 as the particle size decreased almost in half from 528 to 260 µm in Fig. 9. This also suggested that the number of impacts and, therefore, the number of counted peaks in the current-time curves would be increased by eight times as the particle diameter was reduced by a half. However, the figure shows that the number of experimental detectable peaks at the particle size of 260 µm was less than three times (i.e., 320 vs. 120 impacts) of that at the size of 528 µm. The removal of any corrosion products and plastic deformation by the impingement of smaller particles (i.e., with lower impact energy) could be so finite that induced non-detectable peaks in the current–time curves. This resulted in the number of counted peaks to only be 3.6% of the theoretical impacts for a slurry containing particles with a size of 260 µm, whereas, this value was about 11% for the particles with a size of 528 µm.

The mass (or volume) of each particle increases eight times as the diameter is doubled. Knowing that the energy of

each particle is a linear function of the mass, an about eight-fold increase in the energy of each particle was expected as the diameter was almost doubled. It was obtained by Burstein and Sasaki [23] that the current rise was approximately linear with the impact energy of the erodent particles. Therefore, it was expected that the average area under the peaks to increase by eight times as the size of the particle was doubled. Moreover, the larger particles with greater volume could have larger apparent contact area with the eroded surface to generate greater bare metal surface. Therefore, more than eight times increase in the average charge, i.e., the average area under the peaks, induced by each impact would be expected with increasing the particle size from 260 to 528 µm. Figure 9 indicates that the average area under each theoretical expected impact, i.e., obtained by dividing the total charge by the number of theoretical expected impacts increased more than 10 times as the particle size increased from 260 µm to 528 µm. However, an increase of about four times from 1.4 to 5.3 nC in the average area under the detectable peaks, i.e., obtained by dividing the total charge by the number of detectable impacts, was observed as the particle size doubled. As mentioned before, about 94.4% of the impacts could not induce detectable peaks for the particles with a size of 260 µm. This value was 89% for particle size of 528 µm. Therefore, there were more non-detectable current peaks for the smaller particles. These non-detectable peaks, i.e., the particle impacts with a slight effect on the surface that could not generate large enough current to be detected, could not be considered in the calculations. Therefore, the obtained average area under the detectable peaks was inevitably overestimated for both particle sizes. However, the percentage of overestimation of the average area under the peaks for the smaller particles was higher due to the higher number of non-detectable peaks.

The erosion-enhanced corrosion rates (ΔC_w) were obtained from the current–time curves of noise measurements during the erosion-corrosion tests using two particle sizes of 260 µm and 528 µm and are illustrated in Fig. 10. The figure shows an increase of up to 2.8 times in ΔC_w as the particle size increased from 260 to 528 µm at various sand concentrations. A higher increase was obtained at a higher sand concentration. Figure 11 shows the polarization curves and the corrosion current densities of Al-brass alloy at two sand concentrations of 10 and 30 g/l for two particle sizes

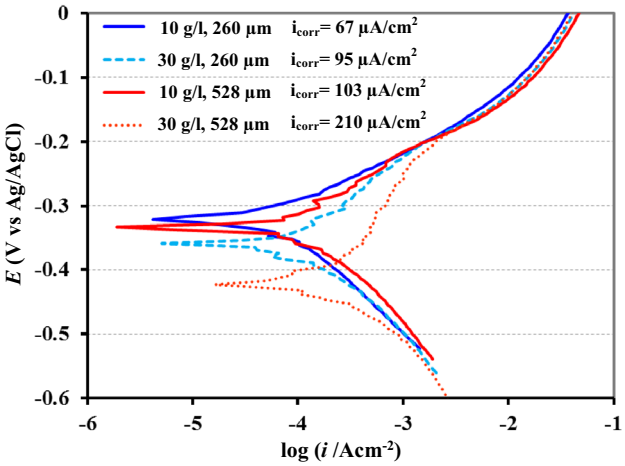

Fig. 11 Polarization curves of Al-brass alloy during the erosion–corrosion process at an impingement angle of 90°, jet velocity of 6 m/s at sand concentrations of 10 and 30 g/l with particle sizes of 260 µm and 528 µm

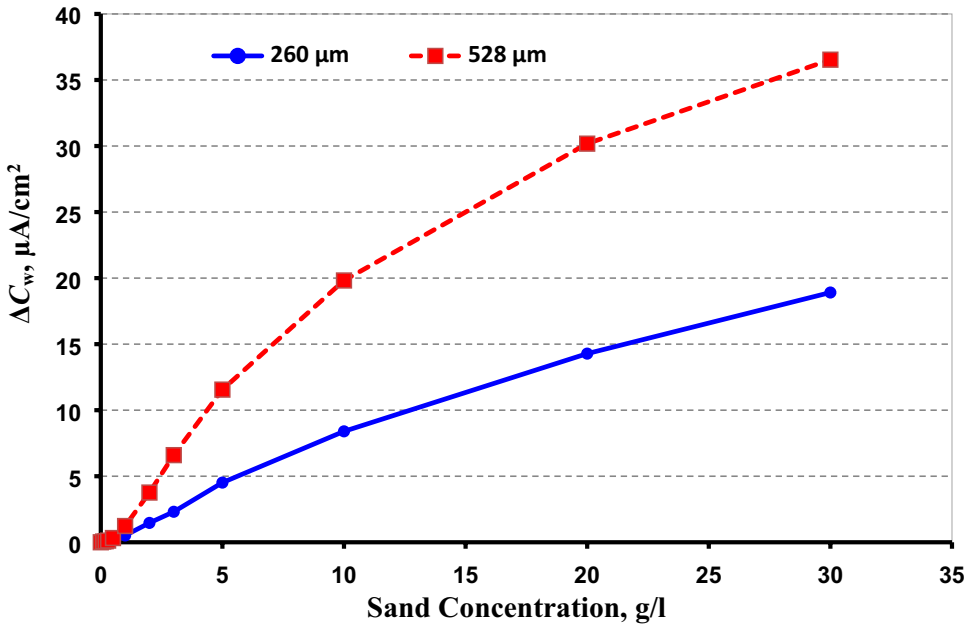

Fig. 10 Erosion-enhanced corrosion current densities (ΔC_w) of Al-brass alloy obtained by electrochemical noise measurements at a jet velocity of 6 m/s, an impingement angle of 90°, the particle sizes of 260 µm and 528 µm as a function of sand concentration

of 260 µm and 528 µm. With increasing the particle size, the corrosion rate of the alloy increased and confirmed the results obtained from the current–time curves of the noise data in Fig. 10. Increasing the particle size at a constant sand concentration decreased the number of the particle impacts and increased the impact energy. These two factors, i.e., the lower frequency of impact and the larger energy of a particle, were in contradiction with the corrosion point of view. The former tried to lower the corrosion current density, whereas, the second factor would increase the corrosion rate during erosion-corrosion by increasing the removal rate of corrosion products and inducing a higher plastic deformation. The results obtained from the noise measurements (Fig. 10) and the polarization curves (Fig. 11) indicated that the corrosion rate of Al-brass alloy has increased as the particle size increased. The effect of increase in the impact energy and volume of each particle with increase in the particle size was larger than the effect of the decrease in the frequency of impacts. The results are not in agreement with the ones obtained in the literature. Niu and Cheng [33] reported that there was no apparent effect on the polarization behavior of 3003 aluminum alloy in solution containing 0.2 g/l sand with various particle sizes of 200 and 600 µm. Rajahram et al. [24] found a lower corrosion current of UNS S31603 for the particle size of 300–600 µm as compared with the size of 150–300 µm. Different designs of erosion rigs were used in the above studies [24, 33], which could be a reason for the dissimilar trend in the erosion-corrosion rate with increasing the particle size as compared with the data presented in this paper. Using a slurry pot [24] or a rotating disk [33] in which the erodent particles retained suspended in the solution by the rotation of the samples could induce some error in studying of the effect of particle size on erosion-corrosion rate. According to Stokes' law [34], as the particle size increased, the settling velocity of particles in a solution increased and a higher number of particles might be deposited at the bottom of the container. Therefore, a lower number of particles were impacted on the surface leading to a lower corrosion rate as the particle size was increased. The slurry impingement rig used in the present study, however, did not induce this type of error in the erosion-corrosion measurements. Therefore, a higher corrosion rate was obtained for the larger erodent particles as shown in Figs. 10 and 11.

4 Conclusions

Two methods of polarization and electrochemical noise were used to investigate the localized and general corrosion behavior of Al-brass alloy under slurry erosion. The eroded surfaces were studied to determine the capability of electrochemical noise for detecting the particle impingements on the surface. The obtained results from the polarization and electrochemical noise methods under various sand concentrations and particles sizes were analyzed and discussed. The results could be concluded as follow:

- SEM study of an eroded surface of Al-brass alloy revealed that the number of particle impacts was close to the theoretical value. However, the number of well-defined peaks in the current–time curves of the electrochemical noise measurements was much lower than the theoretical value. This was related to the impacts with very slight effect on the surface that caused non-detectable current rise in the current–time curves.
- At sand concentrations higher than 10 g/l, the erosion-enhanced corrosion (ΔC_w) obtained from the electrochemical noise were much lower than that from the polarization curves. This implied that the electrochemical noise analysis could not be an accurate method for measuring the erosion-enhanced corrosion of Al-brass alloy at concentrated slurries due to higher possibility of simultaneous impacts and, therefore, overlapping of the current peaks.
- At sand concentrations lower than 10 g/l, the corrosion rate of the alloy obtained by the polarization method did not follow a linear trend. This suggested that the polarization technique was not able to detect the effect of particle impingement on the corrosion behavior of Al-brass alloy during erosion-corrosion. At these conditions the electrochemical noise analysis was a more proper method for measuring the erosion-enhanced corrosion.
- Increasing the particle size at a constant sand concentration led to a decrease in the number of impacts and, therefore, in the number of transient noise current peaks. However, the average area under the noise current peaks was increased resulting in up to 2.8 times increase in erosion-enhanced corrosion as the particle size increased from 260 to 528 µm. The polarization curves also showed an increase in ΔC_w with increase in the particle size.

Compliance with Ethical standards

Conflict of interest On behalf of all authors, the corresponding author states that there is no conflict of interest.

References

1. Aminul Islam M, Farhat ZN (2015) Mechanical and electrochemical synergism of API X42 pipeline steel during erosion-corrosion. J Bio- Tribo-Corros. https://doi.org/10.1007/s40735-015-0027-7
2. Hemmati AR, Soltanieh SM, Masoudpanah SM (2018) On the interaction between erosion and corrosion in chromium carbide

coating. J Bio- Tribo-Corros 4:1–11. https://doi.org/10.1007/s40735-018-0128-1
3. Khayatan N, Ghasemi HM, Abedini M (2017) Synergistic erosion-corrosion behavior of commercially pure titanium at various impingement angles. Wear 380–381:154–162. https://doi.org/10.1016/j.wear.2017.03.016
4. Câmara Noronha L, Velho de Castro V, Ludwig GA et al (2020) Ti–Cp: eletrochemical behaviour under slurry erosion wear. J Bio-Tribo-Corros 7:1–10. https://doi.org/10.1007/s40735-020-00442-y
5. Abedini M, Ghasemi HM (2014) Synergistic erosion—corrosion behavior of Al—brass alloy at various impingement angles. Wear 319:49–55. https://doi.org/10.1016/j.wear.2014.07.008
6. Li Z, Islam MA, Farhat Z (2020) Investigation of erosion-corrosion resistance of electroless Ni–P–Ti composite coatings. J Bio- Tribo-Corros. https://doi.org/10.1007/s40735-020-00404-4
7. Pasha A, Ghasemi HM, Neshati J (2016) Synergistic erosion-corrosion behavior of X-65 carbon steel at various impingement angles. J Tribol 139:011105. https://doi.org/10.1115/1.4033336
8. Azarian NS, Ghasemi HM, Monshi MR (2015) Synergistic erosion and corrosion behavior of AA5052 aluminum alloy in 3.5 wt% NaCl solution under various impingement angles. J Bio-Tribo-Corros 1:10. https://doi.org/10.1007/s40735-015-0010-3
9. Skal S, Kerroum Y, Guenbour A et al (2019) Erosion-corrosion effect on the alloy 316L in polluted phosphoric acid. J Bio- Tribo-Corros. https://doi.org/10.1007/s40735-019-0270-4
10. Abedini M, Ghasemi HM (2016) Corrosion behavior of Al-brass alloy during erosion-corrosion process: effects of jet velocity and sand concentration. Mater Corros 67:513–521. https://doi.org/10.1002/maco.201508511
11. Shi Z, Song G, Cao CN et al (2007) Electrochemical potential noise of 321 stainless steel stressed under constant strain rate testing conditions. Electrochim Acta 52:2123–2133. https://doi.org/10.1016/j.electacta.2006.08.029
12. Monticelli C, Trabanelli G, Mészáros G (1998) Investigation on copper corrosion behaviour in industrial waters by electrochemical noise analysis. J Appl Electrochem 28:963–969. https://doi.org/10.1023/A:1003401128653
13. Girija S, Mudali UK, Raju VR et al (2005) Determination of corrosion types for AISI type 304L stainless steel using electrochemical noise method. Mater Sci Eng A 407:188–195. https://doi.org/10.1016/j.msea.2005.07.022
14. Sanchez-Amaya JM, Cottis RA, Botana FJ (2005) Shot noise and statistical parameters for the estimation of corrosion mechanisms. Corros Sci 47:3280–3299. https://doi.org/10.1016/j.corsci.2005.05.047
15. Homborg AM, Cottis RA, Mol JMC (2016) An integrated approach in the time, frequency and time-frequency domain for the identification of corrosion using electrochemical noise. Electrochim Acta 222:627–640. https://doi.org/10.1016/j.electacta.2016.11.018
16. Suresh G, Mudali UK, Raj B (2011) Corrosion monitoring of type 304L stainless steel in nuclear near-high level waste by electrochemical noise. J Appl Electrochem 41:973–981
17. Haruna T, Morikawa Y, Fujimoto S, Shibata T (2003) Electrochemical noise analysis for estimation of corrosion rate of carbon steel in bicarbonate solution. Corros Sci 45:2093–2104. https://doi.org/10.1016/S0010-938X(03)00031-3
18. Mansfeld F, Sun Z, Hsu CH (2001) Electrochemical noise analysis (ENA) for active and passive systems in chloride media. Electrochim Acta 46:3651–3664
19. Nagiub A, Mansfeld F (2001) Evaluation of corrosion inhibition of brass in chloride media using EIS and ENA. Corros Sci 43:2147–2171
20. Park C, Kwon H (2005) Electrochemical noise analysis of localized corrosion of duplex stainless steel aged at 475 C. Mater Chem Phys 91:355–360. https://doi.org/10.1016/j.matchemphys.2004.11.039
21. Sarmiento H, Goellner J, Heyn A (2010) The influence of the cathodic process on the interpretation of electrochemical noise signals arising from pitting corrosion of stainless steels. Corros Sci 52:1362–1372. https://doi.org/10.1016/j.corsci.2009.12.021
22. Girija S, Mudali UK, Khatak HS, Raj B (2007) The application of electrochemical noise resistance to evaluate the corrosion resistance of AISI type 304 SS in nitric acid. Corros Sci 49:4051–4068. https://doi.org/10.1016/j.corsci.2007.04.007
23. Burstein G, Sasaki K (2001) Detecting electrochemical transients generated by erosion–corrosion. Electrochim Acta 46:3675–3683. https://doi.org/10.1016/S0013-4686(01)00646-6
24. Rajahram SS, Harvey TJ, Wood RJK (2011) Electrochemical investigation of erosion–corrosion using a slurry pot erosion tester. Tribiol Int 44:232–240. https://doi.org/10.1016/j.triboint.2010.10.008
25. Puget Y, Trethewey K, Wood RJ (1999) Electrochemical noise analysis of polyurethane-coated steel subjected to erosion–corrosion. Wear 233–235:552–567. https://doi.org/10.1016/S0043-1648(99)00226-4
26. Mohammadi F, Luo J, Lu B, Afacan A (2010) Single particle impingement current transients for prediction of erosion-enhanced corrosion on 304 stainless steel. Corros Sci 52:2331–2340. https://doi.org/10.1016/j.corsci.2010.03.007
27. Wu PQ, Celis JP (2004) Electrochemical noise measurements on stainless steel during corrosion-wear in sliding contacts. Wear 256:480–490. https://doi.org/10.1016/S0043-1648(03)00558-1
28. Wood RJK, Wharton JA, Speyer AJ, Tan KS (2002) Investigation of erosion–corrosion processes using electrochemical noise measurements. Tribiol Int 35:631–641
29. Abedini M, Ghasemi HM (2017) Erosion and erosion–corrosion of Al-brass alloy: effects of jet velocity, sand concentration and impingement angle on surface roughness. Trans Nonferrous Met Soc China 27:2371–2380. https://doi.org/10.1016/S1003-6326(17)60263-2
30. McCafferty E (2010) Introduction to corrosion science. Springer-Verlag, New York
31. Poggi G (1988) Behaviour of aluminium brass in sea water at various temperatures. Br Corros J 23:122–130
32. Gonzalez-Rodriguez JG, Casales M, Salinas-Bravo VM et al (2004) Electrochemical noise generated during the stress corrosion cracking of sensitized alloy 690. J Solid State Electrochem 8:290–295. https://doi.org/10.1007/s10008-003-0450-4
33. Niu L, Cheng YF (2008) Synergistic effects of fluid flow and sand particles on erosion-corrosion of aluminum in ethylene glycol-water solutions. Wear 265:367–374. https://doi.org/10.1016/j.wear.2007.11.007
34. Gaskell D (2012) An introduction to transport phenomena in materials engineering, 2nd edn. Momentum Press, New York